Research Article | Vol. 9, No. 11 / 1 November 2019 / Optical Materials Express 4370

Optical Materials EXPRESS

Experimental analysis of axial stress distribution in nanostructured core fused silica fibers

Alicja Anuszkiewicz,[1,*] Marek Bidus,[2] Adam Filipkowski,[1] Dariusz Pysz,[1] Michal Dlubek,[2] and Ryszard Buczynski[1,3]

[1] *Department of Glass, Institute of Electronic Materials Technology, Wolczynska 133, 01-919 Warsaw, Poland*

[2] *FIBRAIN Sp. z o.o., Zaczernie 190F, 36-062 Zaczrnie, Poland*

[3] *Faculty of Physics, University of Warsaw, Pasteura 5, 02-093 Warsaw, Poland*

[*] *alicja.anuszkiewicz@itme.edu.pl*

Abstract: We experimentally studied axial stress distribution in recently developed optical all-solid fibers with nanostructured cores. In this type of fiber, the core is composed of thousands of low and high refractive index glass rods with individual diameters of a few hundred nanometers. A distribution of nanorods determines the effective distribution of the refractive index in the core. A structure of nanorods may introduce unrevealed axial stress distribution after fiber drawing, which may induce change of the expected refractive index value. We studied stress in a custom made nanostructured silica fiber with parabolic refractive index distribution in the core and compared it with the reference SMF-28 fiber. For nanostructured fibers we proved that the axial stress is purely thermal with negligible contribution of mechanical stress. This results in the presence of tensile stress in the fiber core, which is in contrary to a standard telecom fiber, where a compressive stress in the core exists. We showed that measured axial stress has negligible impact on refractive index distribution of nanostructured fibers, thus it does not affect its performance.

1. Introduction

Stress present in the optical fiber after drawing is a very important parameter as it changes the refractive index of glass, which in results modifies the optical properties of the fiber. It can also result in surface crack growth [1], which is detrimental to mechanical properties and durability of the fiber [2]. This stress impact on fiber waveguiding and mechanical features has been widely studied for different types of glass optical fibers, polymer optical fibers [3], as well as for semiconductor-in glass structures [4,5] It has been shown, that residual or frozen-in stress is disadvantageous and unwanted in fiber-based devices as it can lead to uncontrollable dispersion or bending losses change [6]. It is also important in Brillouin gain media [7], as it shifts significantly the Brillouin frequency. The residual stress also is considered in long-period grating fabrication, especially with use of arc-discharge, as the stress is released during fabrication process and has adverse impact on LPG forming [8]. On the other hand, frozen-in or residual stress introduced intentionally to the fiber can be very useful, especially in i.e. highly birefringent fibers, which are widely used for sensing [9] and for telecom applications, e.g. PM-fibers [10], as well as in the semiconductor-in glass structures, as it let manipulate band gap structure [5]. To meet the increasing performance demands for the telecommunication, the stress has to be controlled during fiber draw and refractive index changes due to stress presence have to be studied.

The axial stress in fabricated all-solid fibers is well recognized. It strongly depends on drawing force [7], which results in typical stress distributions with tensile stress in the cladding and compressive stress in the core [8]. For photonic crystal fibers (PCFs), to the best of our knowledge, axial stress was not measured as PCFs are made usually of one glass material and there is no

#374796 https://doi.org/10.1364/OME.9.004370
Journal © 2019 Received 7 Aug 2019; revised 22 Sep 2019; accepted 4 Oct 2019; published 17 Oct 2019

Optical Materials EXPRESS

thermal stress caused by differences in glass properties. On the other hand, hole assisted cladding structure of PCF is not suitable for typical axial stress measurement methods, in which use of the immersion with refractive index close to one for fused silica is needed [11]. The axial stress also has not been studied for all-solid PCFs with internal microstructure made of at least two glass materials.

Recently we introduced new type of fiber with nanostructured core (nGRIN fiber). This fiber is made of pure fused silica and germanium doped silica rods arranged as to create effectively parabolic refractive index profile [12]. Such kind of structure allows to modify with the high degree of freedom the propagation properties of optical fiber with preserved compatibility to optical systems working on conventional telecom fibers, i.e. SMF-28 Corning® [13]. However, the core of nGRIN fiber is composed of 2107 rods made of glasses with different refractive indices and different thermal properties. Therefore, as the core structure here is complex and was never earlier studied in terms of axial stress, it can result in unknown axial stress distribution, which can influence the performance of the fiber.

In this work we present for the first time experimental analysis of axial stress distribution in recently introduced new fused silica fiber with nanostructured core [12]. The measurement was performed with use of transverse interferometric method [14] and obtained results were compared with well characterized reference fiber SMF-28. We also analysed the stress origin and its influence on the refractive index profile in the fiber core.

2. Optical fibers and drawing conditions

Fibers considered here are nanostructured graded-index (nGRIN) fibers [12] with effectively parabolic refractive index distribution. A core of nGRIN fiber was composed of two types of glass rods: made of pure silica (a) and germanium doped silica (b). Ge-doped rods (b) were drawn from a step-index preform, in which the core is silica doped with 8.5 %mol of GeO_2 and the cladding is pure fused silica. Simple geometrical calculation allows to estimate effective germanium concentration in Ge-doped glass rod (b), which equals to 4.9 %mol. This assumption is reasonable as the glass rods in the final fiber structure are scaled down to subwavelength sizes and since germanium diffuse into undoped rod area.

To create fiber structural preform, the rods of pure silica and Ge-doped silica with effective 4.9 %mol GeO_2 concentration were stacked accordingly to calculated pattern (Fig. 1a) and thermally integrated. The same structural preform cladded with additional glass cylinder to ensure specific cladding diameter was drawn into structural subpreform and used to draw all fibers considered within this paper as well as those presented in [12]. Resulting structural subpreform size was constant for all fibers and equals to 16.5 mm. Images of pattern, structural preform and one exemplary fiber #3 with zoomed core area are shown in Fig. 1.

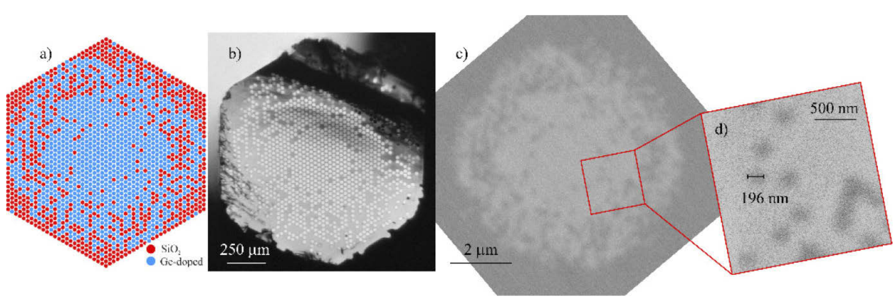

Fig. 1. Design pattern (a) and SEM image (b) of structural preform. SEM images of a core of optical fiber #3 (c) and zoomed core area (d).

Optical Materials EXPRESS

The design pattern was calculated on a basis of effective medium approximation (EMA) [15]. Maximum possible rod diameter in the final fiber was assumed for short wavelength of 633 nm accordingly to EMA condition of $\lambda/3$. This imposed final diameter of nanorod not greater than 211 nm in final fiber. A detailed description of the design and fabrication process of nGRIN fibers is given in [12].

Since Ge doped and undoped silica have different thermal and mechanical properties we can expect that some internal stress can exist in the fiber. For instance, 8.5 %mol Ge-doped silica has thermal expansion coefficient equal to 13.2×10^{-7} K^{-1} [16], which is higher than for pure silica 5.9×10^{-7} K^{-1} [17]. Viscosity close to transition temperature of undoped silica equals to 13.1 dPa s [18], while for doped silica it is lower, but exact value is not accessible in the literature. What is more, as the nGRIN fiber core is made of arbitrarily arranged nanorods distribution of the stress is not obvious and difficult to analyse theoretically. Moreover, diffusion plays important role in this kind of structure, but again is difficult to model. We decided then to investigate the stress distribution experimentally for series of nGRIN fibers.

Geometrical parameters including the core (2r) and cladding (2R) diameters are gathered in Table 1 for all nGRIN optical fibers as well as for the reference fiber SMF-28 [19]. A series of nGRIN fibers was drawn in various conditions as follows: furnace temperature T_f, preform feeding speed v_{feed} and fiber drawing speed v_{draw}. The temperature of furnace was similar and varied from 1960 to 1990 for all drawn fibers. The ratio of fiber drawing rate and preform feeding rate changed between fibers from 17×10^3 to 20×10^3. As the furnace temperature for drawing process for each fiber was comparable, it can be assumed that the drawing tension was the same for all fibers. It is worth to mention that the drawing rate typical in the industry is at the level of 10–20 meters per second, which imposes higher furnace temperatures and feeding velocity to minimize mechanically induced stress.

Table 1. Geometrical parameters and drawing conditions of nGRIN fibers.

	geometrical parameters		drawing conditions			
Fiber	2r [μm]	2R [μm]	T_f [°C]	v_{feed} [mm/min]	v_{draw} [m/min]	v_{draw}/v_{feed} [$\times10^3$]
#1	7.00	125.3	1980	0.25	4.9	20
#2	7.15	125.0	1990	0.57	10.5	18
#3	7.44	135.8	1960	0.26	4.3	17
#4	7.45	128.0	1990	0.62	10.6	17
#5	8.20	134.2	1980	0.26	4.3	17
#6	8.28	132.6	1980	0.26	4.3	17
SMF-28	8.20	125.0	n/a	n/a	n/a	n/a

3. Measurement of axial stress distribution

Residual stress in standard optical fiber is a result of superposition of two stress components: thermally induced stress and mechanically induced stress.

First is caused simply by difference in core and cladding glass thermal expansion coefficients and viscosities and can be assumed as the stress distribution in fiber preform [11]. Thermal stress in the cladding is compressive (negative values) and relatively small. In the core area the stress is tensile (positive values) and moderate [8], because of typically lower viscosity and higher thermal expansion coefficient of germanium doped silica core material.

Mechanically induced stress is introduced to the fiber during drawing process. It has reverse characteristics to one for thermally induced stress and its values depend on drawing force. It dramatically changes resultant stress profile. As the mechanically induced stress typically is dominant, final stress characteristic shows tensile stress in the cladding and compressive stress in

Optical Materials EXPRESS

the core, which results from drawing force and cooling process [19]. Optimization of drawing conditions for the same two material preform enable control over the contribution of mechanical stress to final stress distribution in the fiber. This is advantageous as it allows intentional change of refractive index distribution [7] or enhancement of mechanical properties of the fiber.

The photoelastic effect allows measurement of stress in nondestructive manner. Typically, linearly polarized light illuminates the optical fiber transversely experiencing the phase retardance caused by stress-induced birefringence in the fiber. Finally, retardation measured radially, converted with use of inverse Abel transform [20], permits to determine radial stress distribution. In our study we used commercially available IFA-100 Multiwavelength Optical Fiber Analyzer [21], wich is a standard system for refractive index and axial stress distribution measurement typically used for testing of telecom fibers. This device allows to retrieve phase retardance by spatially resolved extension of Dispersive Fourier Transform Spectroscopy (DFTS) and its accracy is ± 5 MPa for the stress and ± 1×10^{-4} for refractive index measurement [14].

The investigated fibers were stripped of polymer coating, cleaned in an ultrasonic washer and tested with use of fused silica matching liquid (06350 immersion from Cargille Laboratories) [22]. The refractive index of liquid at 633 nm equals to n_{liq}=1.4571 in room temperature (25 °C).

In the first step the reference fiber SMF-28 was investigated to visualize typical axial stress characteristics in single-mode silica fiber. In Fig. 2 the white area without stress corresponds to immersion and is not taken in consideration. The edges of the striped area define diameter of the fiber. On the cladding edges we observe maximum tensile stress of around 11 MPa, which is typical for this kind of fiber and is a result of drawing tension. Uniform grey area indicates position of the core. We observe here typical compressive stress of around −9 MPa, which is caused by later solidification of the core connected with smaller viscosity of germanium doped silica and higher thermal expansion coefficient. The two notches localized symmetrically on the sides of the core are caused by OH impurities introduced to fiber preform at core/cladding boundary. As was mentioned before the measurement error of axials stress for IFA-100 is quite high and equals to ± 5 MPa [21]. Nevertheless, the values are typical and comparable to the results presented in the literature for different measurement techniques (Table 2) and confirm dominant role of mechanically induced stress in SMF-28.

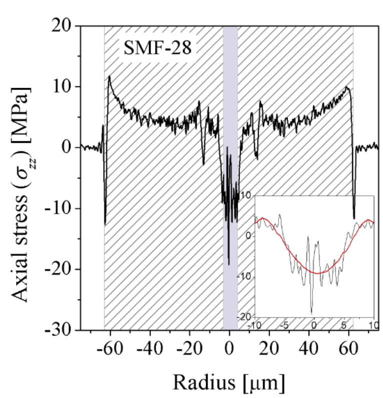

Fig. 2. Axial stress distribution in SMF-28 with indicated core (uniform grey) and cladding (striped grey) areas. Inset shows smoothed compressive stress in the core for estimation of maximum averaged stress value.

The axial stress distribution obtained in the cladding of a standard size fiber (2R = 125 µm) refer to high fiber drawing speed of about 300 m/min, see Fig. 1 in [23]. Except the drawing rate, the other drawing conditions can be assumed as similar, therefore drawing rate is a key parameter which defines mechanical stress distribution in final fiber. Since the drawing rate used

Optical Materials EXPRESS

Table 2. Maximum axial stress values in the core and cladding of SMF-28.

year	reference	maximum stress [MPa]		method
		cladding	core	
1999	[24]	11.3	−10	half-shade
2004	[23]	9.6	−8	optical tomography
2006	[25]	9.91	−10	half-shade
2006	[25]	9.04	−8	quater waveplate
2011	[20]	9.74	−4.4	Brace-Köhler
2011	[19]	10.2	−5.2	Brace-Köhler
2012	[26]	12	−13	Sénarmont
2016	[8]	12	−5	Brace-Köhler
2019	this article	11	−9	DFTS

for fabrication of nGRIN fibers is almost two orders of magnitude smaller (about 5 m/min), than that for SMF-28, the influence of mechanically induced stress should be insignificant and the thermal component should have main contribution to final stress distribution in the fiber.

In the next step we experimentally analysed the axial stress distribution in series of nGRIN fibers with use of the same device IFA-100. The measurement results are depicted in Fig. 3. For all nGRIN fibers identical behaviour of axial stress distribution is observed. Tensile stress is present in the cladding with relatively small value ranging from 2 to 6 MPa. Tensile stress also occurs in the core with moderate value in the range from 19 to 33 MPa (Table 3). Mechanically induced tensile stress in the cladding has very small value, which is observed especially for fibers #1 to #4. For fibers #5 and #6 the contribution of mechanical stress is so low that it compensates only initial thermal stress showing effectively no stress on the cladding edge. It is worth to mention, that the draw tension is mainly sustained for higher viscosity cladding material, which solidifies first. Draw tension has then relatively small impact on core material, which has lower viscosity and solidifies after the cladding.

Table 3. Axial stress values in the cladding (maximum) and in the core (average) of all investigated fibers.

Fiber	2R [μm]	maximum stress [MPa]	
		cladding	core (avg)
#1	125.3	4	23
#2	125.0	3	19
#3	135.8	5	33
#4	128.0	2	21
#5	134.2	3	29
#6	132.6	4	32
SMF-28	125	11	−9

For all fibers the dips of negative stress near the core are visible. It is due to the spatial difference of viscosities between the cladding and core materials, which results in compression stress between the materials boundary after fiber cooling. The stress distribution in the cores is tensile for all fibers. The stress is then reverse to that for reference fiber SMF-28. The reasons for this difference are as follows:

Optical Materials EXPRESS

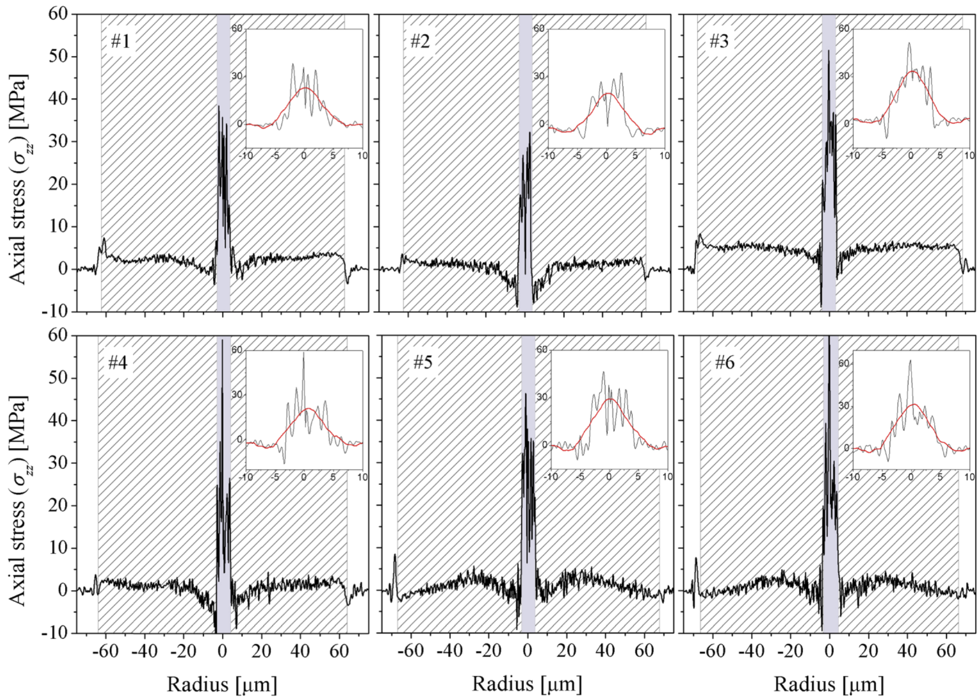

Fig. 3. Axial stress distribution in nGRIN fibers from #1 to #6 with indicated core (uniform grey) and cladding (striped grey) areas. Insets show smoothed tensile stress in the core for estimation of maximum averaged stress value (Table 3).

(a) higher initial thermal stress, caused by higher germanium doped inclusions (smaller viscosity and higher thermal expansion coefficient) in the core of nGRIN fiber in respect to SMF-28;

(b) much smaller drawing speed (drawing tension), e.g. about 5 m/min vs. 300 m/min, respectively for nGRIN fibers and SMF-28, assuming similar remaining drawing conditions.

We observed the described differences also in axial stress distributions represented by 2D stress maps measured for SMF-28 and nGRIN fiber, Fig. 4. For clarity only center of the fiber is depicted, showing most interesting stress change on the core/cladding edge. Compressive stress is present in the core of SMF-28 (blue area with negative values). In the core of nGRIN the stress is tensile (red area with positive values) and its distribution follows the localization of germanium doped inclusions (see core pattern in Fig. 1(b)).

We can observe the stress modulation in the cores of all nGRIN fibers (Figs. 3–4). It is not obvious if the fluctuation is related to the fiber structure, because the character of these modulation is rather resultant from the used measurement method and its limited resolution. In the final fiber individual glass rods in solid core structure have a size of about 200 nm (Fig. 1(d)), while spatial resolution of stress measurement method is around $\lambda/2 \approx 316$ nm [18]. What is more, accordingly with effective medium approximation (EMA) [15], fiber structure is still effective ($\lambda/3.2$) at the wavelength used for axial stress investigations (633 nm). Summarizing, the modulation is visible, but it is difficult to conclude about its origin, as the resolution of the method is too small and similar features can be observed for reference fiber SMF-28 (Fig. 2).

It was indicated earlier that mechanically induced stress has smaller impact on the core than on the cladding. That of course depends on tension value and final stress equilibrium in the fiber. In the case of nGRIN fibers, it can be assumed that as the axial stress in the cladding is

Optical Materials EXPRESS

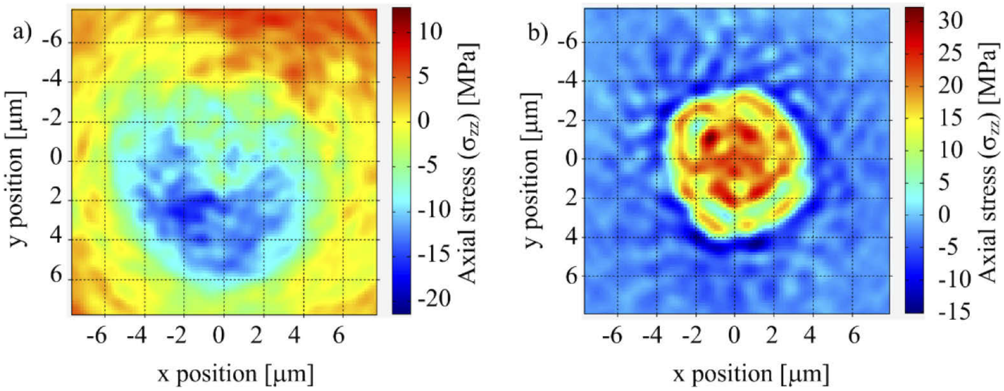

Fig. 4. 2D axial stress map measured for (a) SMF-28 and (b) nGRIN fiber #3.

very small, which confirms small draw tensions, the mechanically induced stress has negligible impact on overall stress characteristic. The axial stress profiles are then close to purely thermal stress distributions, which allows to conclude that final refractive index profiles of nGRIN fibers, are the result of material composition and nanostructure pattern, not affected by stress introduced by drawing.

4. Refractive index distribution

Refractive index distributions of all studied fibers were measured with use of the same device as for stress analysis. IFA-100 allows direct measure of relative phase, which is proccesed using tomographic reconstruction algorithm to calculate final RI distribution [14].

Accordingly with earlier study [12] and due to effective medium approximation, the refractive index distribution that is 'seen' by the light should be continuous and parabolic for nGRIN fibers with maximum contrast equivalent to 4.9 %mol Ge-doped fused silica. From the theory at the measurement wavelength of 633 nm maximal value of RI contrast equals to 7.46×10^{-3} [27]. We have measured RI distribution for fiber #3 and presented the results in Fig. 5. The lowest value of RI corresponds to the pure silica cladding (striped area). In the area outside the fiber we observe the RI level measured for matching liquid (horizontal line in Fig. 5(a)). For the core (uniform grey area) measured maximum RI value equals to $(7.4 \pm 0.2)\times10^{-3}$, which perfectly matches theoretical predictions. To compare the shape of designed and experimentally measured RI profiles we showed zoomed core area of the fiber (Fig. 5(b)) with theoretical approximation (red curve). We calculated the theoretical effective RI profile using Eq. 1 from [12] and theoretical values of RI for pure and 4.9 %mol Ge-doped fused silica. As it can be seen, although the core structure is discrete (see Fig. 1) it produces effectively continuous parabolic RI distribution, which is in good agreement with the theory in the range of measurement error. In Fig. 5(c) we also present 2D map of RI distribution, which shows acceptable uniformity and confirms effective behaviour of the nanostructure even for short wavelength of 633 nm, for which the EMA condition is only $\lambda/3.2$.

Measured RI results are in agreement with the theory, e.g. parabolic RI profile is preserved and maximum value of RI is not affected by axial stress. Moreover, it can be predicted that for the stress at the level of $\pm$ 40 MPa, rough approximation of the stress induced RI change will be at the level of $\pm 2\times10^{-4}$ [28], which is in a range of measurement error for used method. The axial stress values measured for investigated fibers do not exceed $\pm$ 40 MPa and can be neglected as they do not have impact on RI distribution and thus on performance of the fiber.

Optical Materials EXPRESS

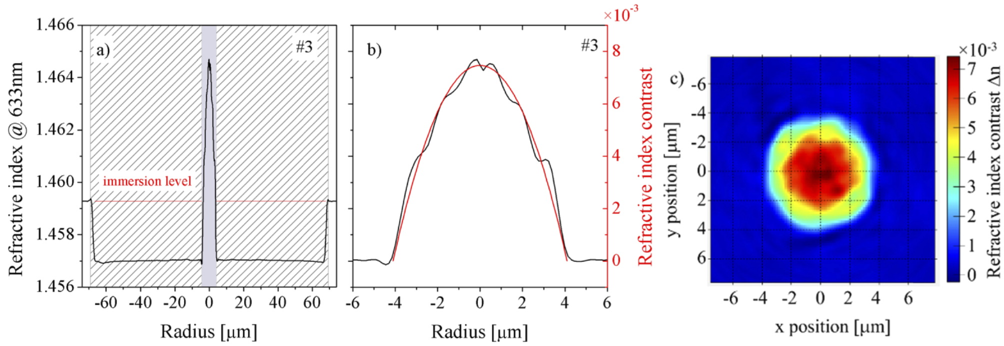

Fig. 5. Refractive index distribution measured at a wavelength of 633 nm in the fiber #3: (a) total profile with indicated immersion, cladding and core area, (b) zoomed core area with parabolic theoretical approximation (red curve) and (c) 2D map of RI contrast in the central part of the fiber (14×14 μm^2).

5. Conclusions

Unknown axial stress distributions were studied for nGRIN optical fibers. As a reference fiber we used SMF-28 in which resultant stress characteristic has dominant mechanical component. Accordingly, in the cladding of SMF-28 the stress is tensile with maximum measured value of 11 MPa, while in the core it is compressive and reaches −9 MPa. The results obtained for nGRIN fibers revealed different origin of axial stress in the fiber core in comparison with SMF-28 and also distributed character. Because of well-balanced drawing conditions the measured stress in the core of all nGRIN fibers has mainly thermal component. Therefore, in the core of nGRIN fiber measured stress is tensile with maximum value ranging between the fibers from 19 to 32 MPa. The stress measured for the cladding of nGRIN fibers is tensile, as in the case of SMF-28. However, its maximum values are smaller (2-5 MPa) than for SMF-28, which confirms lower drawing speeds. Measured stress values in the fiber cores do not exceed ± 40 MPa. For this level of stress roughly estimated change of the refractive index equals to 2×10^{-4}, which is less than 0.02 % of the refractive index, thus measured stress has negligible impact on fiber performance.

Stress analysis was followed by measurement of refractive index profile for nGRIN fibers. Obtained results show effectively continuous parabolic profile of RI, which is in perfect match with the design and theoretical predictions. This also confirms that the residual stress has negligible impact on resultant refractive index characteristic and that the fiber performance is preserved.

Within this paper the origin of an axial stress present in nGRIN fibers was revealed. The obtained results confirm that even for such a complex structure in the core there is no unexpected phenomena causing disadvantageous change in performance of the nGRIN fiber. As there is no additional limitations caused by residual stress, this kind of structures can be considered for future research and development, which would open new directions for progress in telecommunication fibers and fiber optics-based devices.

Funding

Fundacja na rzecz Nauki Polskiej (POIR.04.04.00-1C74/16).

Acknowledgments

The authors thank Waclaw Urbanczyk for fruitful discussion and indication of unknown distribution of frozen-in stress in a complex core structure of nGRIN optical fibers.

Optical Materials EXPRESS

References

1. P. L. Chu and T. Whitbread, "Stress modification in optical fibre," Electron. Lett. **20**(11), 449–450 (1984).
2. P. C. P. Bouten, W. Hermann, C. M. G. Jochem, and D. U. Weichert, "Drawing influence on the lifetime of optical fibres," J. Lightwave Technol. **7**(3), 555–559 (1989).
3. M. K. Szczurowski, T. Martynkien, G. Statkiewicz-Barabach, W. Urbanczyk, L. Khan, and D. J. Webb, "Measurements of stress-optic coefficient in polymer optical fibers," Opt. Lett. **35**(12), 2013–2015 (2010).
4. D. A. Coucheron, M. Fokine, N. Patil, D. W. Breiby, O. T. Buset, N. Healy, A. C. Peacock, T. Hawkins, M. Jones, J. Ballato, and U. J. Gibson, "Laser recrystallization and inscription of compositional microstructures in crystalline SiGe-core fibres," Nat. Commun. **7**(1), 13265 (2016).
5. M. Fokine, A. Theodosiou, S. Song, T. Hawkins, J. Ballato, K. Kalli, and U. J. Gibson, "Laser structuring, stress modification and Bragg grating inscription in silicon-core glass fibers," Opt. Mater. Express **7**(5), 1589–1597 (2017).
6. W. Hermann, M. Hutjens, and D. U. Wiechert, "Stress in optical waveguides. 3: Stress induced index change," Appl. Opt. **28**(11), 1980–1983 (1989).
7. Y. Sikali Mamdem, E. Burov, L-A. de Montmorillon, F. Taillade, Y. Jaouën, G. Moreau, and R. Gabet, "Importance of residual stresses in the Brillouin gain spectrum of single mode optical fibers," in *Proceedings of IEEE 37th European Conference and Exhibition on Optical Communication* (IEEE, 2011), pp. 1–3.
8. P. Wang, M. H. Jenkins, and T. K. Gaylord, "Arc-discharge effects on residual stress and refractive index in single-mode optical fibers," Appl. Opt. **55**(9), 2451–2456 (2016).
9. A. Anuszkiewicz, T. Martynkien, P. Mergo, M. Makara, and W. Urbanczyk, "Sensing and transmission characteristics of a rocking filter fabricated in a side-hole fiber with zero group birefringence," Opt. Express **21**(10), 12657–12667 (2013).
10. D. Dobrakowski, A. Rampur, G. Stepniewski, A. Anuszkiewicz, J. Lisowska, D. Pysz, R. Kasztelanic, and M. Klimczak, "Development of highly nonlinear polarization-maintaining fibers with normal dispersion across entire transmission window," J. Opt. **21**(1), 015504 (2019).
11. P. K. Bachmann, W. Hermann, H. Wehr, and D. U. Wiechert, "Stress in optical waveguides. 2: Fibers," Appl. Opt. **26**(7), 1175–1182 (1987).
12. A. Anuszkiewicz, R. Kasztelanic, A. Filipkowski, G. Stepniewski, T. Stefaniuk, B. Siwicki, D. Pysz, M. Klimczak, and R. Buczynski, "Fused silica optical fibers with graded index nanostructured core," Sci. Rep. **8**(1), 12329 (2018).
13. Corning SMF-28® technical note: http://www.corning.com/media/worldwide/coc/documents/Fiber/PI1463_07-14_English.pdf
14. A. D. Yablon, "Multi-Wavelength Optical Fiber Refractive Index Profiling by Spatially Resolved Fourier Transform Spectroscopy," J. Lightwave Technol. **28**(4), 360–364 (2010).
15. A. Sihvola, *Electromagnetic Mixing Formulas and Applications Institution of Electrical Engineers*, London, UK (1999).
16. P. K. Bahman, D. U. Wiechert, and T. P. M. Meeuwsen, "Thermal expansion coefficients of doped and undoped silica prepared by means of PCVD," J. Mater. Sci. **23**(7), 2584–2588 (1988).
17. Heraeus data sheet: "High purity fused silica tubes for optical fiber production tubes," https://www.heraeus.com/media/media/hcv/documents/products_and_solutions_11/High_purity_fused_silica_tubes_EN.pdf
18. Heraeus data sheet: "Base materials," https://www.heraeus.com/media/media/hca/doc_hca/products_and_solutions_8/BaseMaterials_Image_EN.pdf
19. M. R. Hutsel, PhD thesis: https://smartech.gatech.edu/bitstream/handle/1853/42926/hutsel_michael_r_201112_phd.pdf
20. M. R. Hutsel, R. R. Ingle, and T. K. Gaylord, "Technique and Apparatus for Accurate Cross-Sectional Stress Profiling of Optical Fibers," IEEE Trans. Instrum. Meas. **60**(3), 971–979 (2011).
21. IFA-100 application note: http://www.amstechnologies.com/fileadmin/amsmedia/downloads/5103_refractiveindexmeasurementonopticalfiber.pdf
22. Cargill matching gel data sheet: https://cargille.com/wp-content/uploads/2018/07/Fused-Silica-Matching-Liquid-Code-06350.pdf
23. Y. Park, U.-C. Paek, S. Han, B.-H. Kim, C.-S. Kim, and D. Y. Kim, "Inelastic frozen-in stress in optical fibers," Opt. Commun. **242**(4-6), 431–436 (2004).
24. K. W. Raine, R. Feced, S. E. Kanellopoulos, and V. A. Handerek, "Measurement of axial stress at high spatial resolution in ultraviolet-exposed fibers," Appl. Opt. **38**(7), 1086–1095 (1999).
25. C. C. Montarou, T. K. Gaylord, and A. I. Dachevski, "Residual stress profiles in optical fibers determined by the two-waveplate-compensator method," Opt. Commun. **265**(1), 29–32 (2006).
26. G. Violakis, N. Aggarwal, and H. G. Limberger, "Stress changes in H2-loaded SMF optical fibers induced by cw-Ar + 244 nm irradiation," Opt. Mater. Express **2**(11), 1490–1495 (2012).
27. J. W. Fleming, "Dispersion in GeO_2-SiO_2 glasses," Appl. Opt. **23**(24), 4486–4493 (1984).
28. Schott technical information: https://www.us.schott.com/d/advanced_optics/1275dc1e-ef01-45d1-a88a-79deec322443/1.2/schott_tie-27_stress_in_optical_glass_us.pdf